# The dynamics of travertine terraces

Ø. Hammer[1], D. K. Dysthe[1], B. Jamtveit[1]

[1]PGP - Physics of Geological Processes, University of Oslo, PO Box 1048 Blindern, 0316 Oslo, Norway

**Travertine (limestone) terraces are common in caves[1], springs[2-4] and rivers[5-6] worldwide, and represent one of the most striking examples of geological pattern formation on the Earth's surface. The terraces form over a wide range of scales, from millimeters to tens of meters (Figs. 1A, D). Their origin has been poorly understood, but most likely involves a coupling between the precipitation rate and hydrodynamics. Microbial activity may also play a role[2]. Here we present a minimal model based on shallow-water flow and an empirical positive correlation between the flow velocity and precipitation rate. The resulting self-organizing pattern formation process displays rich and unusual dynamics, consistent with field observations. Terraces coarsen with time, fold into lobes and migrate downstream with differential rates, resulting in striking patterns. This model, in which topography grows rather than erodes in response to rapid flow, produces patterns that are completely different from those generated by flow driven erosion.**

The formation of travertine deposits is driven primarily by evaporation of carbon dioxide from carbon dioxide rich water that has dissolved calcium carbonate in the subsurface. On gradual slopes, a series of terraces is formed (Fig. 1A) but well-defined terraces do not form on steep slopes with fast, chaotic flow (Fig. 1B). The temporal development of travertine terraces can be deduced from cross sections. Excellent sections are available in the quarries at Rapolano Terme, Italy[4]. The cross-sections show development of terraces from an initially smooth surface, downstream step migration, coarsening due to drowning by higher downstream terrace edges, and downstream thinning of wedge-shaped layers on the outer rim wall[4] (Fig. 1C). At Rapolano Terme, step coarsening eventually leads to the recurrence of large-scale topographic smoothness. Although these spectacular structures clearly result from elevated precipitation rates at terrace edges (rims) and vertical faces, the mechanism for this differential rate is less obvious. Current views favor one or both of the following: (1) enhanced precipitation under higher flow velocity because of thinning of a diffusion-limiting boundary layer[5,7]; (2) accelerated degassing of $CO_2$ due to agitation, pressure drop and shallowing[1, 8]. Although these mechanisms are probably important, other processes such as sticking of particles to the rim[9] possibly enhanced by biofilms, and ballistic deposition with shadowing effects[10] could also contribute. We do not address here the mechanism for differential precipitation in these systems. Rather, we accept the empirical relationship between flow velocity and precipitation rate observed by several authors[5-6]. Through simulation and comparison with field observations we investigate whether such a relationship is sufficient to produce terraces, and, if so, how they grow and evolve in time.

A simple computer model based on a linear relationship between flow velocity and precipitation rate was used to simulate the pattern growth process. The simulation runs in alternate steps: (1) the steady state water flow is calculated for the current topography; and (2) the topography is updated based on the flow velocity controlled precipitation rate. We used the code Hydro2de[11] for depth-averaged shallow 2D flow. The rate of elevation change is given by

$$\frac{\partial z}{\partial t} = D\nabla^2 z + max\left(f(u), a\right)\sqrt{1+(\nabla z)^2}$$

where $z(x,y)$ is the topographic elevation and $\mathbf{u}(x,y)$ is the flow velocity. $D$ is a diffusion coefficient for particle transport, and $f$ is a precipitation scaling factor. The term $\sqrt{1+(\nabla z)^2}$ converts growth normal to the surface into vertical growth. The influence of flow on precipitation is limited by the parameter $a$. This model resembles the KPZ equation[12], which can be interpreted as a general surface-normal growth model, except that growth is controlled by the flow velocity and there is no stochastic term. The growth step is implemented using an explicit scheme on the same grid as the hydrodynamic model, with grid size $h$=0.1m and time step $\Delta t$=1 day. We used $D$=1.0*10$^{-5}$ m$^2$/day, $f$=10$^{-3}$ s/day, and $a$=10$^{-3}$ m/day. For $|\boldsymbol{u}|$ ranging from 0 to 1 m/s, this gives growth rates from 0 to 1 mm/day, comparable with natural rates (30 cm/year has been measured locally within the Mammoth Hot Springs, Yellowstone[3]). The computational domain size is 20 by 20 meters, with a 10 l/s point-source inflow in the middle of one edge, and free outflow along the opposite edge. The initial topography is a flat slope dropping 2 m from inflow to outflow, with small uncorrelated initial random perturbations. Bed friction follows the Manning law[13] with $n$=0.033.

Fig. 2 shows a typical run. Initially, a mound forms around the inlet, grading into a distal apron. The reduction in velocity as flow spreads laterally causes reduced precipitation rate and reduced slope away from the source (cf. Fig. 1B). Further downslope, the initial random perturbations reorganize into closely spaced small scale terraces, starting as short, irregular ridges, parallel or oblique to strike. Their initial spacing is influenced by the simulation grid size (0.10 m). Water flows along a ridge until it reaches its end, and then resumes free downslope flow. Therefore, precipitation is fast along a ridge but also at the ends of ridges, causing them to elongate. With time, the ridge nuclei straighten and coalesce in a general orientation along strike, resulting in a mature small scale terrace. Small terraces coarsen over time, developing into larger terraces and pools that flood smaller upstream pools. On the proximal mound or chimney, terraces do not form, because the flow velocity exceeds 1 m/s and is not rate limiting for precipitation (because of the maximum growth rate, $a$).

Rims migrate downslope without dissolution on the inner side of the terrace, due to the difference in precipitation rate on the inner and outer sides which causes the rim to grow upwards and outwards. This process is shown clearly in cross sections (Fig. 3). The faster growth associated with larger rims results in a larger absolute difference in precipitation rate between the inner and outer side, causing larger rims to migrate faster and overtake smaller downstream terraces. This process, contributing to coarsening, is reminiscent of 'step bunching' in crystal growth[14]. Another effect of rim migration is an instability causing formation and expansion of lobate pools (fingering). In any small initial pool, rim migration will proceed in the local downstream direction, causing outward expansion. The general slope of the terrain implies larger step size at the downslope tip of the pool than at the sides, which can produce a differential rim migration rate and a downslope stretching of the pool. On very steep slopes, fingering is weaker because the gradient is controlled by the underlying slope. The steepness at the outer face of large terraces generally hinders further small scale fingering.

The pattern is stable with respect to perturbation. If an incision is made in a rim, flow is diverted away from the rest of the edge and is concentrated to the notch. Precipitation then ceases at the dry edge, but is amplified in the incised channel, filling it until the horizontal rim is restored. Conversely, placing an object on a rim will divert flow around it, restoring the rim. Such regeneration of shape is likely to contribute to the regularity of natural travertine steps even when perturbed by breakage, deposition of large particles, and biological activity.

The morphological complexity makes it difficult to define and measure pool size. One crude approach is to study the distribution of terraces along a one-dimensional transect in the general downslope direction. The transect will cut pools at random lateral positions, and only occasionally where the size is maximal. Still, such analysis indicates periodicity and hence a dominant pool size. Spectral analysis (Supplementary Fig. 1) shows a dominant spectral peak corresponding to a period of about 8 grid cells (80 cm). This periodicity may partly stem from homogeneous coarsening of the initial grid-controlled small terrace size, but similar periodicity is also found in nature (Supplementary Fig. 2).

For better understanding of the basic geometric and hydrodynamic relationships, the model is intentionally minimal and based on a simple empirical relationship. However, travertine growth rates clearly depend not only on local flow velocity, but also on larger-scale downstream development of water chemistry under degassing and precipitation[15]. A more complete simulation should include reaction, transport and degassing of chemical species, coupled with a carbonate precipitation model. In addition, field observations indicate that surface tension, which is not included in the present model, is a critical parameter controlling flow in thin films over small terraces.

The flow velocity in natural systems depends in a complex manner on the surface topology, and it is correlated with variables such as the water depth. Therefore, the success of our model does not show that the flow velocity is the causal factor controlling precipitation rate, since flow velocity and precipitation rate could both result from water depth or some other quantity. However, we have shown that a simple model based on the coupling of precipitation rate and flow velocity is sufficient for terrace formation, and we have investigated the resulting pattern formation dynamics. In addition, theoretical and experimental work[1,7,8,16] indicates that the flow velocity can indeed act as a direct causal control on precipitation rate, at least under turbulent flow conditions. Other mechanisms may enhance the positive feedback on step edges and the resulting instability.

Coarsening is the fundamental dynamic feature. There is no stable characteristic wavelength, like that found in ice terrace models[17-19]. From field observations, we speculate that a stable wavelength can emerge if surface tension is included in the model[18]. However, at any given time the step distance in the simulation is relatively constant, as shown by spectral analysis. Informally, we ascribe this to the competition between two fundamental processes: local self-enhancement (positive feedback) of step edges through the flow velocity/precipitation rate coupling, and lateral inhibition by upstream flooding. The inhibition range is controlled by step size, as larger

steps will flood larger upstream regions. This general situation is a familiar recipe for self-organization into regular spacing of features, for example in reaction-diffusion models[20]. Clearly, the range of upstream inhibition of terrace formation by flooding is inversely proportional to slope, giving closer spacing of terraces on steep slopes, a commonly observed feature of travertine deposits.


1. Varnedoe Jr, W. W. A hypothesis for the formation of rimstone dams and gours. *Bull. Natl. Speleol. Soc.* **27**, 151-152 (1965)
2. Chafetz, H. S. & Folk, R. L. Travertines: depositional morphology and the bacterially constructed constituents. *J. Sediment. Petrol.* **54**, 289-316 (1984)
3. Fouke, B. W. *et al.* Depositional facies and aqueous-solid geochemistry of travertine-depositing hot springs (Angel Terrace, Mammoth Hot Springs, Yellowstone National Park, U.S.A.). *J. Sed. Res.* **70**, 565-585 (2000)
4. Guo, L. & Riding, R. Hot-spring travertine facies and sequences, Late Pleistocene, Rapolano Terme, Italy. *Sedimentology* **45**, 163-180 (1998)
5. Zaihua, L., Svensson, U., Dreybrodt, W., Daoxian, Y. & Buhmann, D. Hydrodynamic control of inorganic calcite precipitation in Huanglong Ravine, China: Field measurements and theoretical prediction of deposition rates. *Geochim. Cosmochim. Acta* **59**, 3087-3097 (1995)
6. Lu, G., Zheng, C., Donahoe, R. J. & Lyons, W. B. Controlling processes in a $CaCO_3$ precipitating stream in Huanglong Natural Scenic District, Sichuan, China. *J. Hydrol.* **230**, 34-54 (2000)
7. Buhmann, D. & Dreybrodt, W. The kinetics of calcite dissolution and precipitation in geologically relevant situations of karst areas. 1. Open system. *Chem. Geol.* **48**, 189-211 (1985)
8. Chen, J., Zhang, D. D., Wang, S., Xiao, T. & Huang, R. Factors controlling tufa deposition in natural waters at waterfall sites. *Sediment. Geol.* **166**, 353-366 (2004)
9. Eddy, J., Humphreys, G. S., Hart, D. M., Mitchell, P. B. & Fanning, P. Vegetation arcs and litter dams: similarities and differences. *Catena* **37**, 57-73 (1999)
10. Meakin, P., *Fractals, scaling and growth far from equilibrium* (Cambridge Univ. Press, Cambridge, 1998)
11. Beffa, C. *Praktische Lösung der tiefengemittelten Flachwassergleichungen* (Mitteilung 133, Versuchsanstalt für Wasserbau, ETH Zürich, 1994)
12. Kardar, M., Parisi, G. & Zhang, Y.-C. Dynamic scaling of growing interfaces. *Phys. Rev. Lett.* **56**, 889-892 (1986)
13. Brater, E. F., King, H. W., Lindell, J. E. & Wei, C. Y. *Handbook of hydraulics*, 7th ed. (McGraw-Hill, New York, 1996)
14. Kandel, D. & Weeks, J. D. Step motion, patterns and kinetic instabilities on crystal surfaces. *Phys. Rev. Lett.* **72**, 1678-1681 (1994)
15. Hammer, O., Jamtveit, B., Benning, L. G. & Dysthe, D. K., Evolution of fluid chemistry during travertine formation in the Troll thermal springs, Svalbard, Norway. *Geofluids* **5**, 140-150 (2005)
16. Liu, Z. & Dreybrodt, W. Dissolution kinetics of calcium carbonate minerals in $H_2O$-$CO_2$ solutions in turbulent flow: the role of the diffusion boundary layer and the slow reaction $H_2O+CO_2 \rightarrow H^+ + HCO_3^+$. *Geochim. Cosmochim. Acta* **61**, 2879-2889 (1997)
17. Ogawa, N. & Furukawa, Y. Surface instability of icicles. *Phys. Rev. E* **66**, 041202 (2002)
18. Ueno, K. Pattern formation in crystal growth under parabolic shear flow. *Phys. Rev. E* **68**, 021603 (2003)
19. Ueno, K. Pattern formation in crystal growth under parabolic shear flow. II. *Phys. Rev. E* **69**, 051604 (2004)
20. Meinhardt, H. *The algorithmic beauty of sea shells* (Springer, Berlin, 1995)


**Supplementary Information** is linked to the online version of the paper at www.nature.com/nature


**Acknowledgements** Hans Amundsen introduced us to the problem and organized field work in Svalbard. Paul Meakin suggested improvements to the manuscript. The work was supported by the Norwegian Research Council.

**Author Contributions** Ø. H. developed the model. All authors performed field work in Svalbard. D.K.D carried out field work in Italy. D. K. D. and B. J. performed field work in Yellowstone. All authors contributed ideas.

**Author Information** Reprints and permission information is available at npg.nature.com/reprintsandpermissions. The authors declare no competing financial interests. Correspondence should be addressed to Ø. H. (ohammer@nhm.uio.no).

**Figure Legends**

Figure 1. (A) Travertine terraces, Minerva Spring, Yellowstone National Park, USA. Delayed precipitation gives a flat top. (B) Orange Mound, Yellowstone. Immediate precipitation produces a proximal dome and a distal apron. Well-formed terraces do not form on the steep surfaces. (C) Cross section of travertine sequence at Rapolano Terme, Italy. Flow was from right to left. From an initially smooth surface (bottom), terraces form, coarsen and migrate downstream. Drowning events D and rim migration M are indicated. (D) Small terraces in the Troll springs, Svalbard, Norway. General flow direction from upper right to lower left.

Figure 2. Days 2000, 4000 and 6000 of the simulation. 20x20 m domain. Lighted from the right. Inflow at the center of upper edge, free outflow along lower edge. Note the formation of a mound around the inlet, and coarsening of downslope terraces. Lower right: Detailed, oblique view, day 6000, water-filled.

Figure 3. Cross sections from the distal apron at simulation time increments of 400 days, illustrating coarsening. Axes in meters. Elevated precipitation rate at outer side of steps, causing downslope step migration, is evident. Cases of upstream drowning of steps are also seen.

**Supplementary figures**

Supplementary Figure 1. Lomb periodogram (spectral analysis) of detrended downslope transect in simulation day 400. The dominant spectral peak around 0.12 cycles per grid point, corresponding to a period of roughly 8 grid points (80 cm) is significant relative to a $p$=0.01 white noise line shown. The splitting of the main peak reflects the non-constant amplitude of the cycle.

Supplementary Figure 2. Lomb periodogram (spectral analysis) of detrended contour through a section at Rapolano Terme, Italy, with a sample spacing of 0.28 cm. The dominant spectral peak is found at 0.00704 cycles per sample, giving a period of 39.8 cm. An additional low-frequency peak reflects a single cycle through the transect.


Fig 1a


Fig 1b

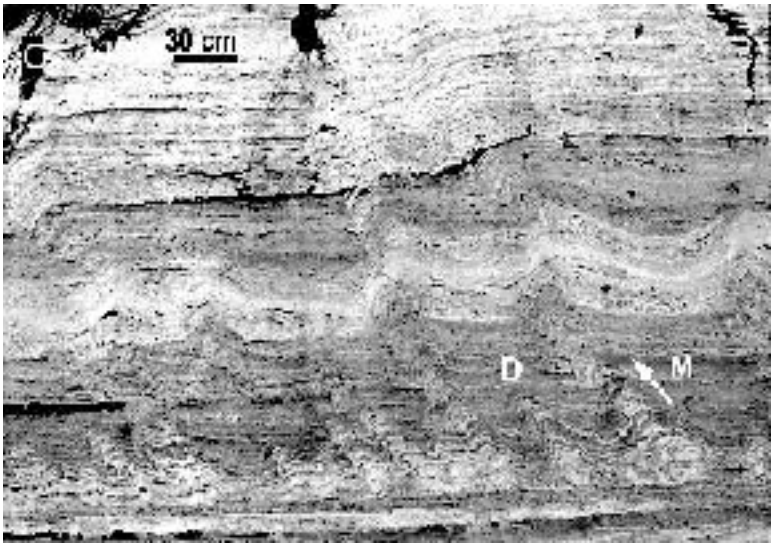


Fig 1c

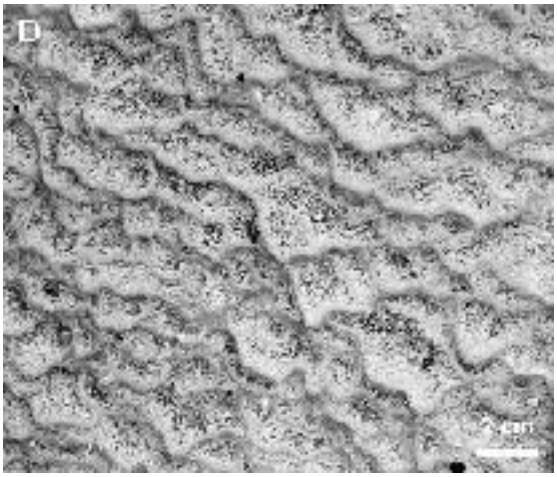


Fig 1d

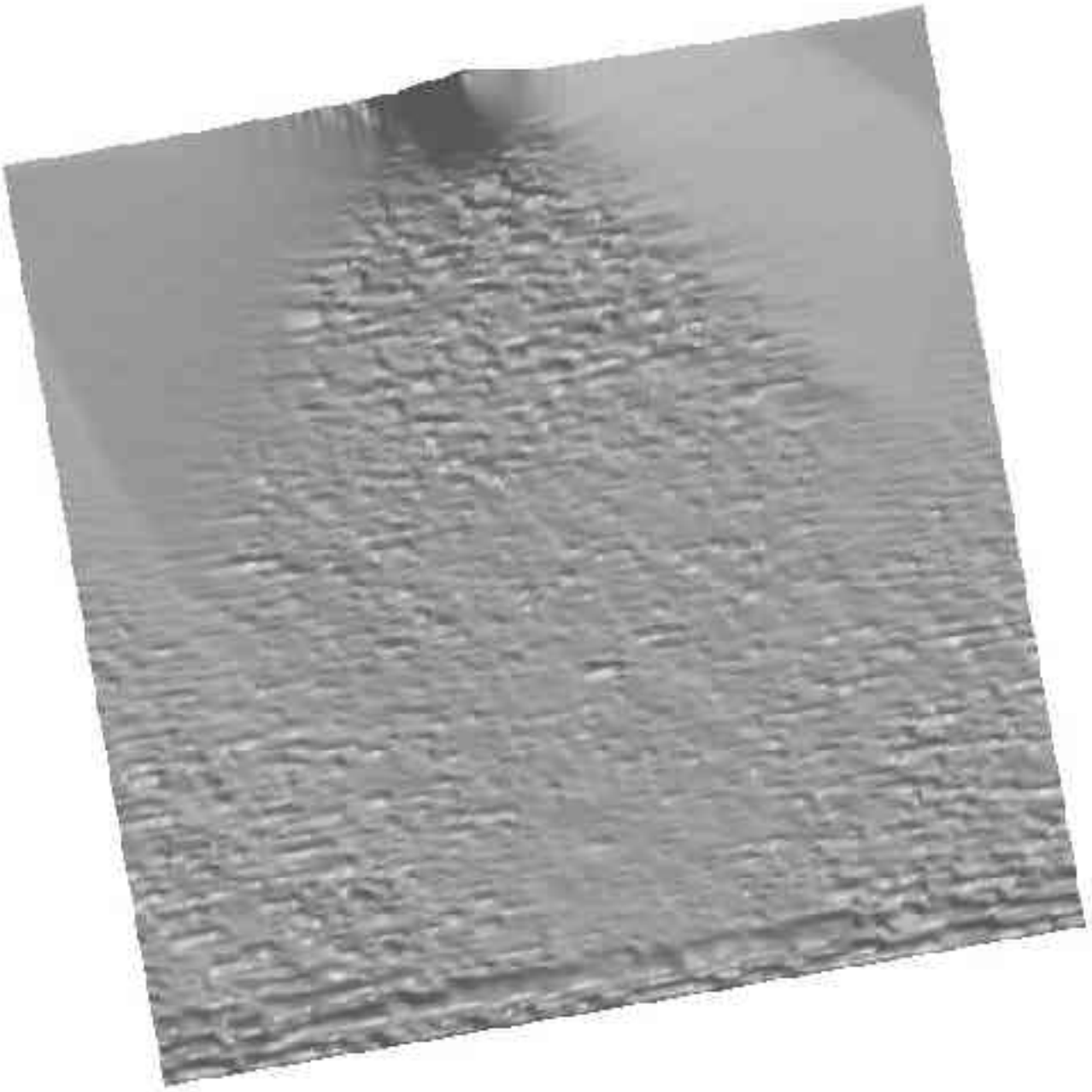

Fig 2a

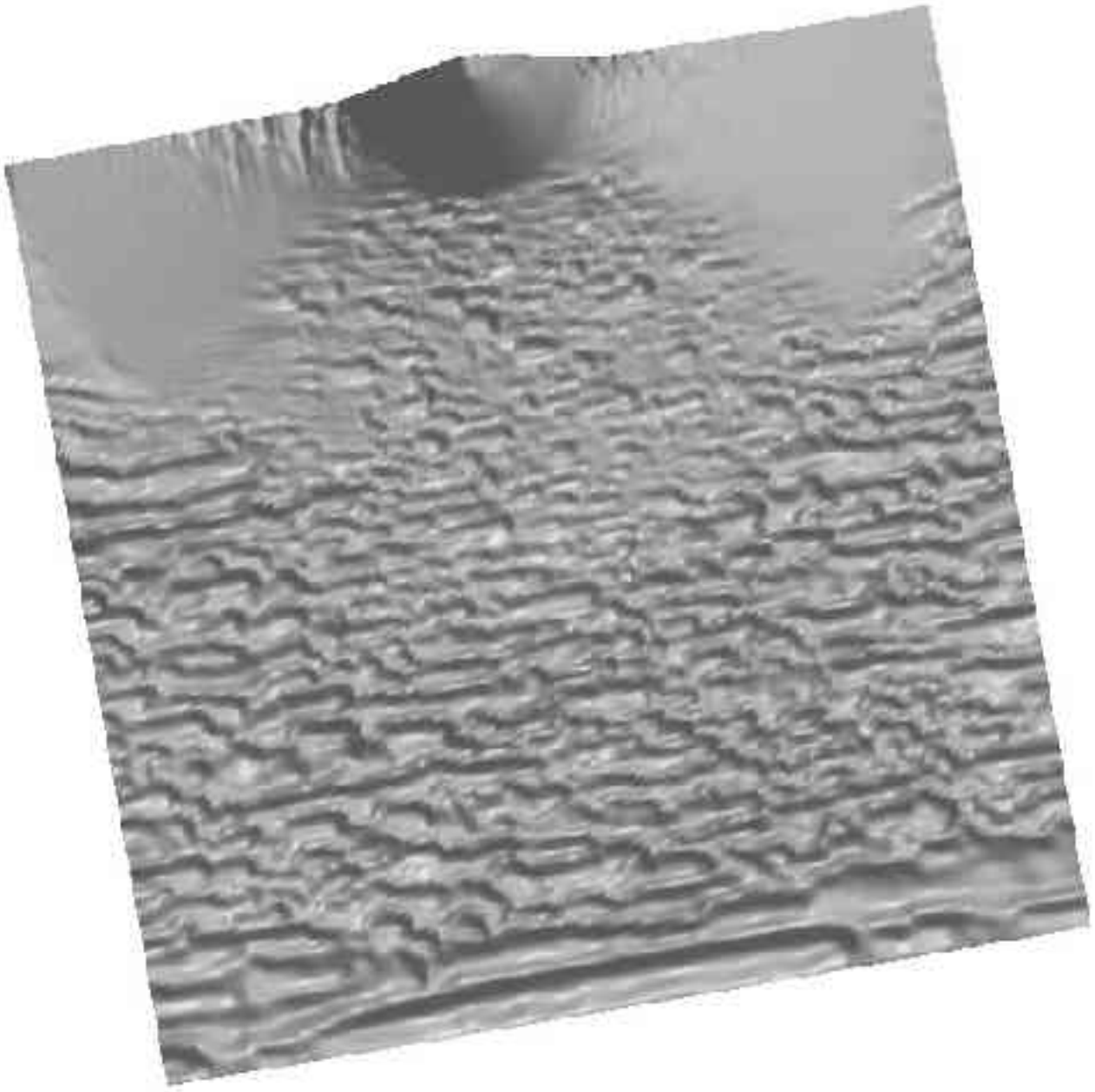

Fig 2b

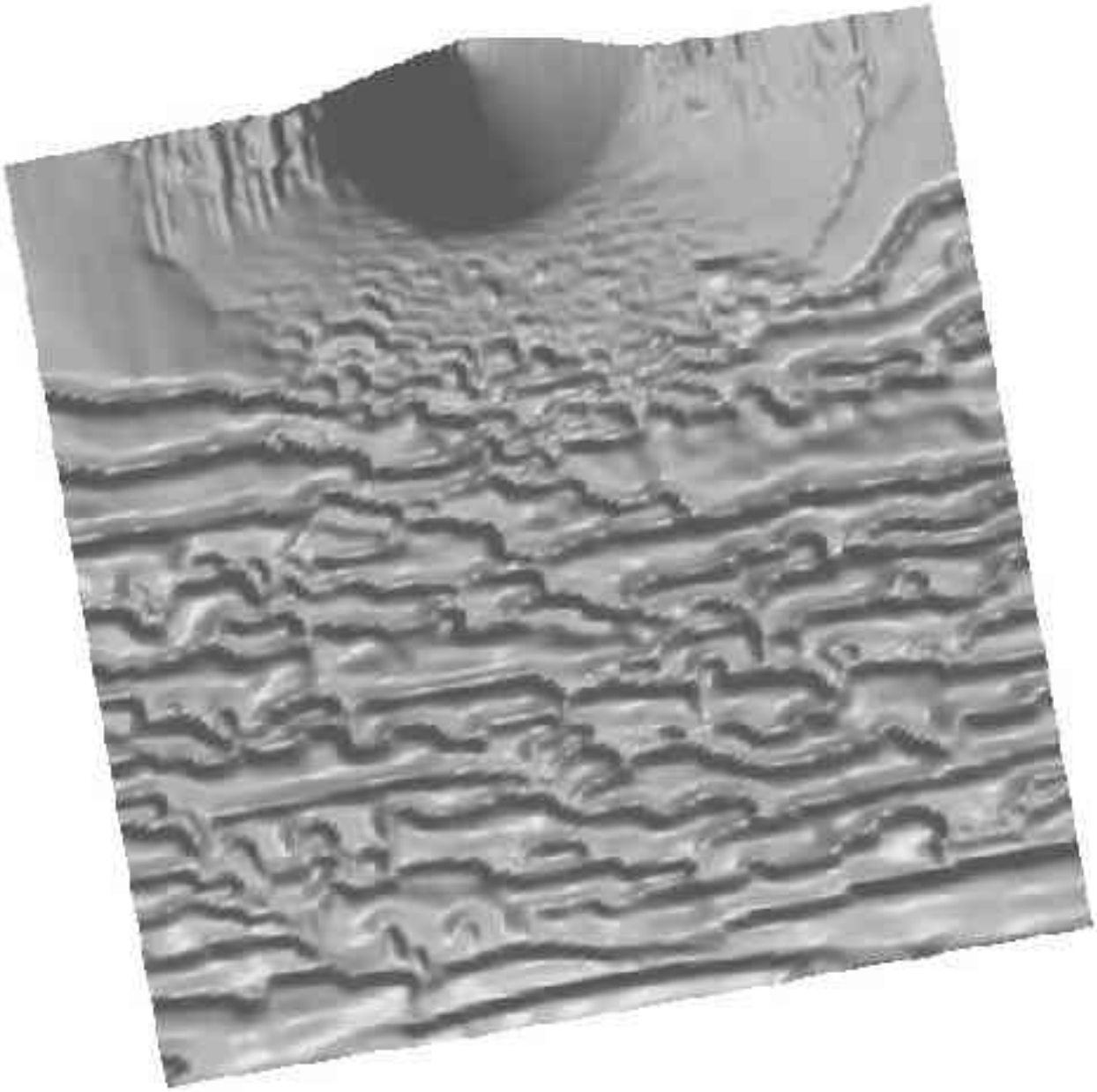

Fig 2c

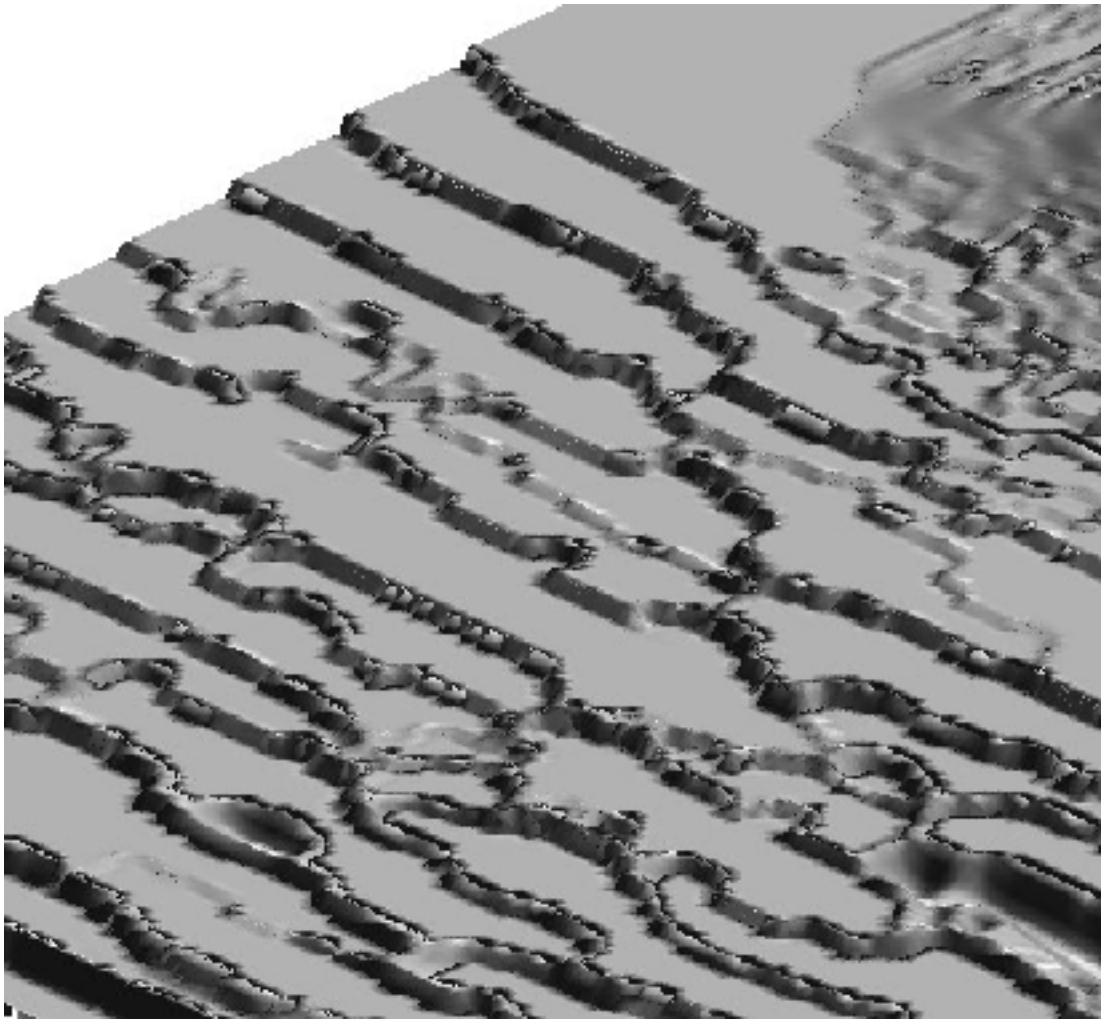

Fig 2d

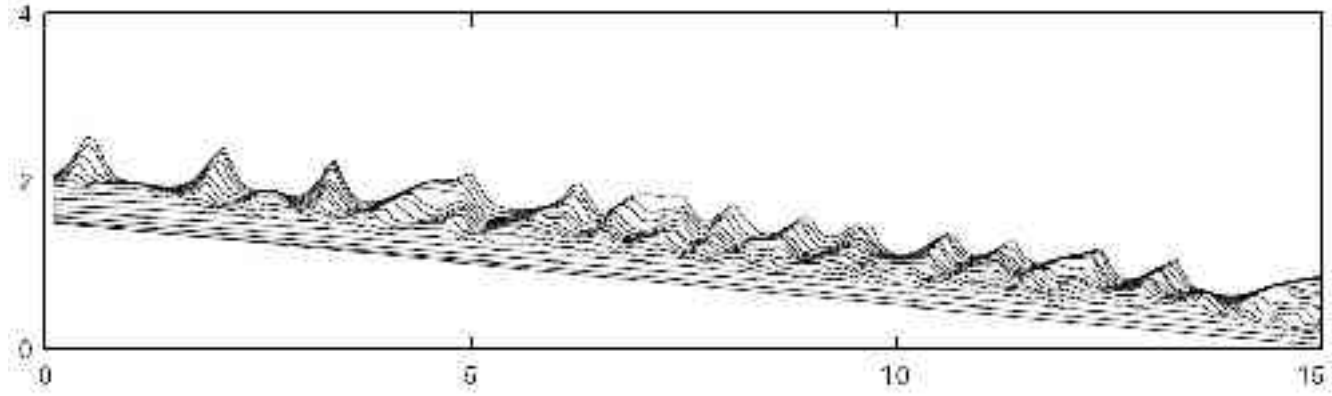


Fig. 3

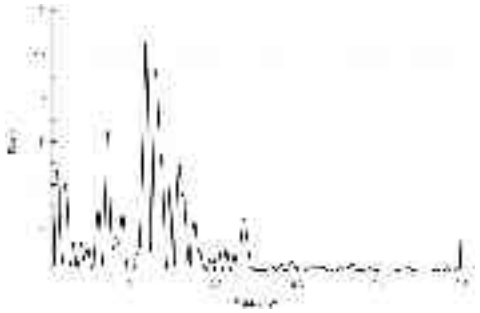

Sup. fig 1

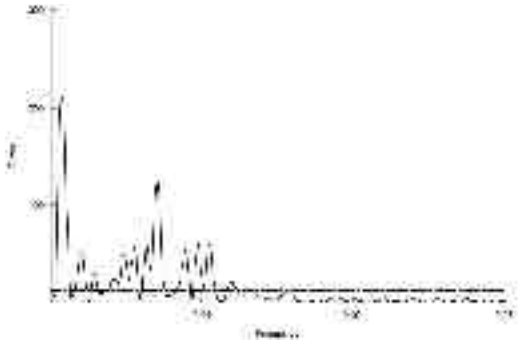

Sup. fig 2